Lateral distributions of EAS muons (Eμ > 800 MeV) measured with the KASCADE-Grande Muon Tracking Detector in the primary energy range 10 16- 10 17 eV

Lateral distributions of EAS muons (E_μ >800 MeV) measured with the KASCADE-Grande Muon Tracking Detector in the primary energy range 10^{16} eV – 10^{17} eV

W.D. Apel[a], J.C. Arteaga-Velázquez[b], K. Bekk[a], M. Bertaina[c], J. Blümer[a,d], H. Bozdog[a], I.M. Brancus[e], E. Cantoni[c,f,1], A. Chiavassa[c], F. Cossavella[f,2], K. Daumiller[a], V. de Souza[g], F. Di Pierro[c], P. Doll[a], R. Engel[a], J. Engler[a], B. Fuchs[f], D. Fuhrmann[h,3], A. Gherghel-Lascu[e], H.J. Gils[a], R. Glasstetter[h], C. Grupen[i], A. Haungs[a], D. Heck[a], J.R. Hörandel[j], D. Huber[d], T. Huege[a], K.-H. Kampert[h], D. Kang[d], H.O. Klages[a], K. Link[d], P. Łuczak[k,*], H.J. Mathes[a], H.J. Mayer[a], J. Milke[a], B. Mitrica[e], C. Morello[f], J. Oehlschläger[a], S. Ostapchenko[a,4], N. Palmieri[d], M. Petcu[e], T. Pierog[a], H. Rebel[a], M. Roth[a], H. Schieler[a], S. Schoo[a], F.G. Schröder[a], O. Sima[l], G. Toma[e], G.C. Trinchero[c], H. Ulrich[a], A. Weindl[a], J. Wochele[a], J. Zabierowski[k,*]

[a] *Institut für Kernphysik, KIT - Karlsruher Institut für Technologie, Germany*
[b] *Universidad Michoacana, Instituto de Física y Matemáticas, Morelia, Mexico*
[c] *Dipartimento di Fisica, Università degli Studi di Torino, Italy*
[d] *Institut für Experimentelle Kernphysik, KIT - Karlsruher Institut für Technologie, Germany*
[e] *Horia Hulubei National Institute of Physics and Nuclear Engineering, Bucharest, Romania*
[f] *Osservatorio Astrofisico di Torino, INAF Torino, Italy*
[g] *Universidade São Paulo, Instituto de Física de São Carlos, Brasil*
[h] *Fachbereich Physik, Universität Wuppertal, Germany*
[i] *Department of Physics, Siegen University, Germany*
[j] *Deptartment of Astrophysics, Radboud University Nijmegen, The Netherlands*
[k] *National Centre for Nuclear Research, Department of Astrophysics, Łódź, Poland*
[l] *Department of Physics, University of Bucharest, Bucharest, Romania*

Abstract

The KASCADE-Grande large area (128 m^2) Muon Tracking Detector has been built with the aim to identify muons (E_μ^{thr}=800 MeV) in Extensive Air Showers by track measurements under 18 r.l. shielding. This detector provides high-accuracy angular information (approx. 0.3°) for muons up to 700 m distance from the shower core. In this work we present the lateral density distributions of muons in EAS measured with the Muon Tracking Detector of the KASCADE-Grande experiment. The density is calculated by counting muon tracks in a muon-to-shower-axis distance range from 100 m to 610 m from showers with reconstructed energy of 10^{16} eV – 10^{17} eV and zenith angle $\theta < 18°$. In the distance range covered by the experiment, these distributions are well described by **Greisen functions**. They are compared also with the distributions obtained with the KASCADE scintillator array (E_μ^{thr}=230 MeV) and with distributions obtained using simulated showers.

Keywords: cosmic rays, extensive air showers, KASCADE-Grande, Muon Tracking Detector, lateral distributions, muon density

1. Introduction

Investigations of the muonic component in extensive air showers (EAS) is of primary importance for understanding air shower physics. Muons carry nearly undistorted information about their parent particles, pions and kaons. These parent particles are the most numerous products of hadronic interactions responsible for the development of the shower cascade in the atmosphere. This longitudinal development contains the information on the nature (mass) of the primary cosmic ray particle, which is related to astrophysical questions. It also carries information relevant to particle physics on the underlying properties of hadronic interactions in the energy range and the kinematical region only recently being accessed by the forward detectors of the LHC [1]. Therefore, study of the mass composition of cosmic rays and the tests of various hadronic interaction models are in many cases related to the investigation of this longitudinal development of showers.

The most common way used by all EAS experiments with sufficient number of muon detectors is the investigation of lateral distributions of muons, being **a projection** of the development of the muonic component onto **the shower plane** [2, 3]. This is usually measured with arrays of scintillation detectors, where the number of muons in each detector is derived from the energy deposited in the scintillators, using non-trivial procedures based on simulations [4, 5].

Muon tracking detectors, actually counting muons in EAS,

*Corresponding authors
Email addresses: luczak@zpk.u.lodz.pl (P. Łuczak), janzab@zpk.u.lodz.pl (J. Zabierowski)

[1] now at: Istituto Nazionale di Ricerca Metrologia, INRIM, Torino
[2] now at: DLR Oberpfaffenhofen, Germany
[3] now at: University of Duisburg-Essen, Duisburg, Germany
[4] now at: Stanford University (CA)

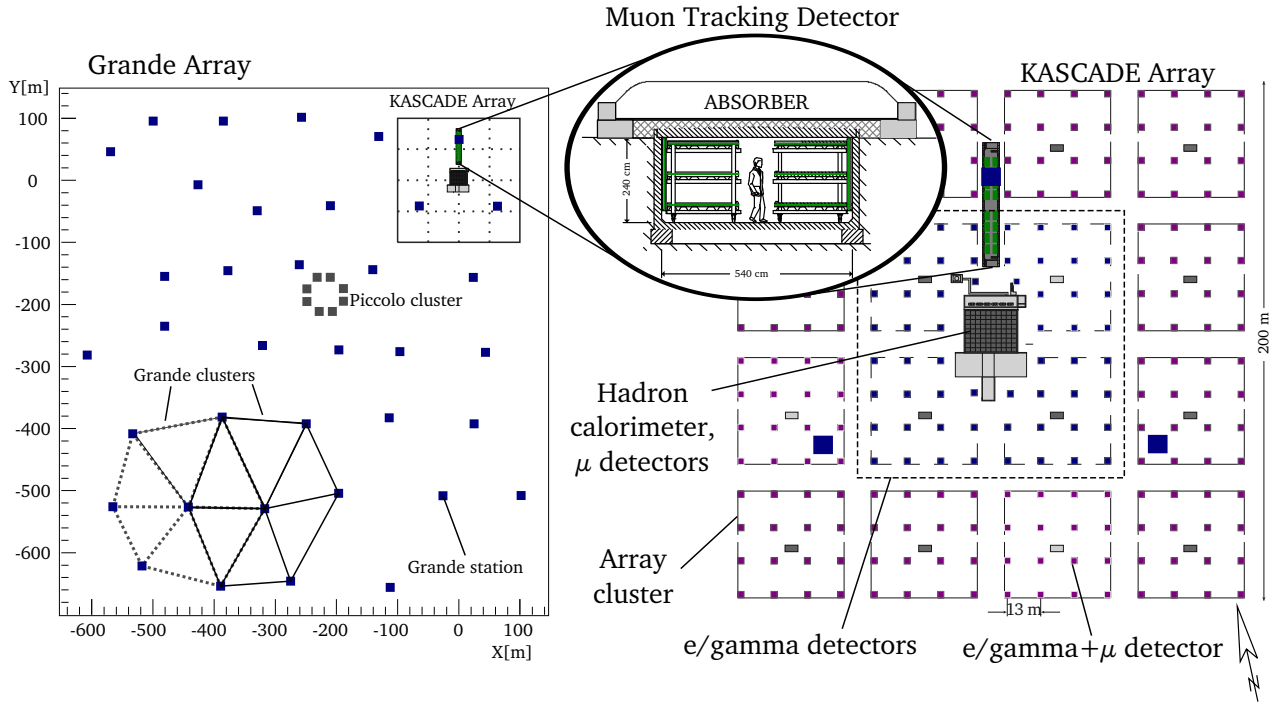

Figure 1: Layout of the KASCADE-Grande experiment. Note the location of the Muon Tracking Detector (MTD) within the KASCADE Array.

have rather not been used for this purpose due to the difficulty of building sufficiently large detectors of this type. Earlier attempts were based on neon flash tubes, either in tracking [6] or hodoscopic [7] configurations. Muon densities were measured close to the shower core (< 30 m in Ref. [7] and 5 m – 70 m in Ref. [6]), and for shower sizes corresponding to the 'knee' region of the primary energy spectrum, around 10^{15} eV. A possibility of the investigation of muon tracks from more energetic showers at larger distances has been created in the KASCADE-Grande EAS experiment [8], being an extension of the KASCADE experimental setup [9]. It is a multi-detector system (Fig. 1) located on the site of the Karlsruhe Institute of Technology (KIT) – Campus North, Germany at 110 m a.s.l. It was designed to detect the three EAS particle components: hadrons, electrons and muons (at 4 energy thresholds) in a wide range of distances from the shower core (up to 700 m), and for primary particle energies from 5×10^{14} eV to 10^{18} eV. High precision measurements of particle densities and tracks – the latter by means of a dedicated Muon Tracking Detector (MTD) [10] – at different energy thresholds allow investigation of many features of EAS and are the basis for multi-parameter analyses (e.g.: [4, 11]).

In particular, the MTD gives a possibility to study the longitudinal development of EAS. For the first time it was possible to investigate the lateral distribution of muons using the muon tracks in a distance up to several hundred meters from the core from a large number of showers with energies above 10^{16} eV. The results of this investigation are reported in this work.

2. Muon tracking in KASCADE-Grande

The KASCADE-Grande experiment (Fig. 1) contains several detector systems. First, it consists of the KASCADE experimental setup located in the North-East corner, where the MTD is also situated. A detailed description of this part of the experiment and its performance can be found elsewhere [9]. In view of the research presented here, apart from the MTD, an array of 252 detector stations (called the *KASCADE Array*), covering an area of 200 m × 200 m, is an important part of the setup. The stations are placed on a square grid with 13 m spacing and are organized in 16 clusters. Each station is equipped with scintillation counters registering the electromagnetic shower component (E^{thr}=5 MeV), and in the outer 12 clusters, also the muonic part of EAS (E^{thr}_{μ}=230 MeV).

A second major part of KASCADE-Grande is the *Grande Array*, being an extension of the KASCADE Array. It consists of 37 detector stations organized in a **grid of 18 clusters of overlapping hexagons**, covering an area of 0.5 km^2 [8]. In the centre there is a small trigger array of plastic scintillation stations, called *Piccolo*, built to provide additional fast triggers for some of the KASCADE detector components.

2.1. Design of the MTD

The MTD is located in the northern part of the KASCADE Array (as shown in Fig. 1) and houses 16 muon telescopes made of *streamer tubes* (ST). The telescopes are placed in a $5.4 \times 2.4 \times 44$ m^3 concrete tunnel, additionally buried under an absorber made of iron plates separated with sand. This shielding corresponds to an equivalent of 18 radiation lengths and

absorbs most of the low-energy electromagnetic particles, thus allowing the identification of the tracks from muons with an energy larger than 800 MeV. The streamer tubes in each muon telescope are grouped in four 2×4 m^2 *detector modules*, three horizontal and one vertical (Fig. 1). The horizontal modules are separated by 820 mm. The middle module is located 1.7 m below the level of the KASCADE scintillator array. The total area for detection of vertical muons is 128 m^2.

All telescopes are connected with a gas supply system, high voltage and electronic chain readout system. An extended description of the design, performance and tests of the MTD can be found in Refs. [10], [12] and [13].

When a particle is passing through the modules of the telescope it ionizes the gas in the streamer tubes and charge-streamers are created. As a result a large increase of charge in a small volume of the tube occurs. This charge is inducing a certain charge in the aluminum *strips* above and below the tubes (perpendicular and diagonal, 30° with respect to the *wires* in the ST), respectively (Fig. 2). A coincidence of the signals from wires and strips in each layer is called a *hit*. The tracks are reconstructed of three or two hits, in three or two modules, respectively.

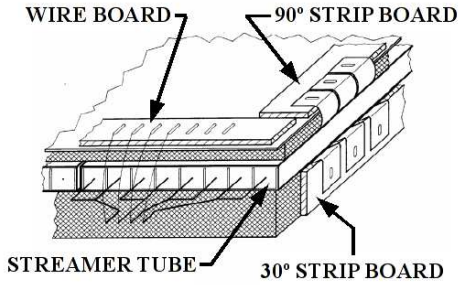

Figure 2: The MTD module design. The PVC boards for fixing signal outputs from wires and strips are shown.

2.1.1. Reconstruction of the muon tracks

From the raw data the information about signals on wires, diagonal and perpendicular strips is retrieved and converted into positions of each wire and strip. The *hit cluster sizes*[5] along the wires and strips (in cm) are reconstructed for each detector module. The position, where the particle crossed the module is estimated as the centre of the cluster and becomes the position of a hit.

Using all hits, the algorithm is searching for hits that can create a track whose direction is correlated with the direction of the shower within an angle of 15°. The 3-hit tracks are reconstructed first. The procedure is then repeated for 2-hit tracks but only for hits that are not involved in 3-hit tracks. The hits that do not fit to any track are ignored.

At muon densities higher than ~0.5 muons/m^2 clusters may overlap and not all tracks are reconstructed or are reconstructed

[5]Number of wires and strips having signal in each hit used in a track reconstruction is called a hit cluster size.

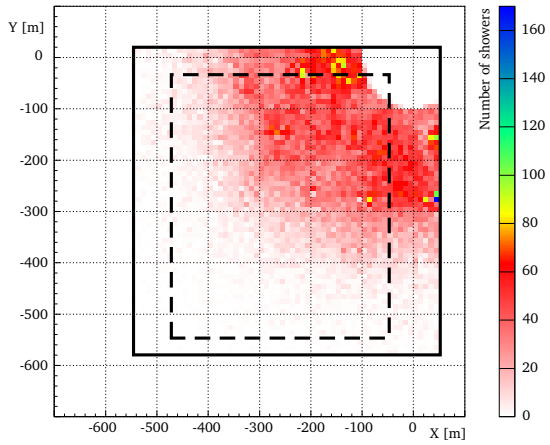

Figure 3: Shower core distribution over the fiducial area used in the MTD analysis (solid-line rectangle). The standard fiducial area (dashed-line rectangle) used in KASCADE-Grande EAS analyses is shown for comparison. **The co-ordinates shown are ground co-ordinates and the point 0,0 is the centre of KASCADE.**

with poor quality [10]. This reconstruction inefficiency occurs when showers fall too close to the MTD. At extreme cases none of the muon tracks are reconstructed. The minimum distance to the shower core where there is still full reconstruction efficiency increases with shower energy. A more detailed description of the detector response can be found in Refs. [10] and [13].

3. Selection of the data

3.1. Selection of experimental showers

This work is based on more than 45 million showers registered with the KASCADE-Grande experiment from November 2003 to June 2009.

Showers selected for the MTD analysis fulfill general conditions used in the KASCADE-Grande analyses (described in Ref. [8]) and the shower zenith angle is less than 18° to avoid registration problems **due to the growing hit cluster sizes** and the effects of the attenuation of muons originating from more inclined showers. The analysis is done for showers with reconstructed primary energy above 10^{16} eV where KASCADE-Grande provides full detection and reconstruction efficiency for $\theta < 18°$.

The energy of each shower is calculated with the formula:

$$\begin{aligned} \lg(E_0^{rec}[GeV]) &= [a_H + (a_{Fe} - a_H) \cdot k] \cdot \lg(N_{ch}) \\ &+ b_H + (b_{Fe} - b_H) \cdot k \end{aligned} \quad (1)$$

$$k = \frac{\lg(N_{ch}/N_\mu) - \lg(N_{ch}/N_\mu)_H}{\lg(N_{ch}/N_\mu)_{Fe} - \lg(N_{ch}/N_\mu)_H} \quad (2)$$

The formula (**see Ref. [14] for details**) is based on the number of charged particles, obtained with the KASCADE (E^{thr}**=5 MeV**) and Grande (E^{thr}**=3 MeV**) arrays, and the number of muons (E^{thr}**=230 MeV**) obtained with the KASCADE Array muon detectors **[8]**. The energy assignment is defined

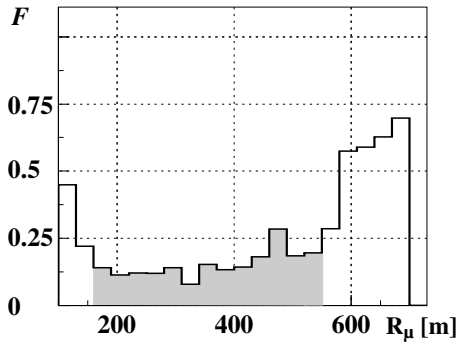

Figure 4: Example of the fraction F of showers triggered by KASCADE Array but without reconstructed muon tracks as a function of muon-to-shower-axis R_μ for the primary energy range $\lg(E_0^{rec}[\mathrm{GeV}])=7.6-7.9$. The region with constant F (plateau) within one standard deviation is indicated with the grey area.

as E=$f(N_{ch}, k)$, where N_{ch} is the size of the charged particle component **(total number of charge particles at observation level)** and the parameter k is defined through the ratio **of the size of the charged component (N_{ch}) and muon size (N_μ), being a total number of muons at the observation level**. The parameters a and b are obtained by Monte Carlo simulations (QGSJet-II-2+FLUKA) and are optimized for the energy and zenith angular range of interest for the present analysis.

The MTD registration is fully efficient in a certain distance range to the shower core. Close to the core the track reconstruction efficiency is affected by the high density of muons that create overlapping hit clusters, and the saturation of the data acquisition system. At larger distances, where the muon density becomes smaller, the registered number of showers with at least one muon is further reduced by trigger and registration inefficiency effects[6] (see Ref. [13]). This leads to the core distribution of showers available for the investigation in the MTD shown in Fig. 3. **The structures observed in this 10 m×10 m binning have no influence on our results what has been checked by calculating muon densities also with removed most deviated areas.** Most of the showers are located within the standard KASCADE-Grande fiducial area around the centre of the Grande Array (dashed-line rectangle). To enlarge statistics of the number of showers with muons used in the MTD analysis it was necessary to increase this area (solid-line rectangle). This extension, however, has no influence on the quality of reconstructed showers used in the MTD analysis.

In the sample of showers passing all selection criteria and having KASCADE trigger in each distance bin there is a number of showers not having muons in the MTD (N_{s0}). **There are two possibilities of such a situation. One is that the density of muons in the shower is too low to give a muon track in the 128 m^2 detector. If so, then such cases should enter into the density calculations with their *empty* areas. The other explanation is the inefficiency of track reconstruction and/or inefficiency of the MTD trigger. Such cases can be treated like "faulty/switched-off detector" and not being considered in the muon density calculations. We have checked both possibilities by investigating the dependence of the fraction of such showers F = N_{s0}/N_{st} on the muon-to-shower-axis distance (R_μ), where N_{st} is the total number of selected showers in a distance bin. An example of such dependence of this fraction for $\lg E_0^{rec}$ interval equal to 7.6 - 7.9 is shown in Fig. 4. At small distances, where the muon density is the largest, the rise of the F value indicates the detector saturation and track reconstruction problems while at large distances trigger inefficiencies seem to be more pronounced. In the plateau region F is constant within one standard deviation, being on the same level of 0.15±0.05 in all primary energy intervals. It is despite the fact that muon density becomes reduced 10 times over that region, shown in gray in Fig. 4. Moreover, examination of all showers without muons did not show any difference between their characteristics and the characteristics of the showers with muons in the MTD. In addition, the Poisson probability of having zero muons in the 128 m^2 detector in the showers with the mean muon track number: 50 at 200 m down to 5 at 560 m is negligibly small. All of this points to the explanation of the showers without muons rather by the experimental reasons than by the physical ones (fluctuations towards lower muon densities).** Therefore, in the plateau region of the F dependence we treat such cases in a similar way like those when the MTD was not operating and for the following analyses only showers N_s, with muon tracks, are taken into account.

3.2. Selection of muons

The standard set of parameters used in the description of muon directions obtained with the MTD contains:
a) coordinates of the point where the muon track crosses the plane of the KASCADE scintillator array, *b*) azimuth and zenith angles of the track, *c*) hit cluster size, *d*) the track pattern describing which modules were involved in the track reconstruction.

Due to the reconstruction inefficiency effects it was necessary to restrict the muon-to-shower-axis distance (R_μ), calculated from the shower core position obtained with the Grande Array and the track position in the shower coordinate system, to be larger than 100 meters.

3.3. Analysis of the simulated data

In the standard KASCADE-Grande simulation set, EAS were simulated with CORSIKA [15] using QGSJet-II-2 [16] as a high-energy and FLUKA2002.4 [17] as a low-energy interaction models. Showers were simulated for H, He, C, Si

[6] The MTD is triggered by the KASCADE Array. The showers detected far away from the KASCADE centre not always generate a KASCADE trigger. Moreover, in such showers, the delay of the KASCADE trigger signal reaching the MTD may be too large for fully efficient registration of all muons reaching the MTD.

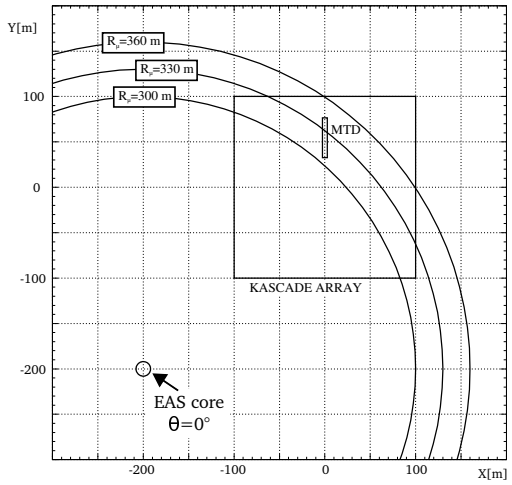

Figure 5: Distance between the muon track and the shower axis R_μ is divided into 30-meter bins. In each bin the number of muon tracks and the area of the MTD are calculated **for each event**.

and Fe primaries with an energy spectrum E^{-2} in the energy range from 10^{14} eV to 10^{18} eV and in the zenith angle range $0^\circ - 42^\circ$.

In the standard simulation set, due to the location of the MTD within the experiment and the relatively small detection area, as well as the higher muon energy threshold, the number of simulated events with muon tracks was too small for statistically significant comparisons with the experimental data. To overcome this problem and to lessen the bias in parameter values created by multiple use of CORSIKA simulated showers a special set of proton and iron initiated showers was generated with a QGSJetII+FLUKA model combination. Showers were simulated only up to 20° in zenith angle and each shower was in the detector simulations used 5 times only over the fiducial area used in the MTD analysis.

In the following analysis, the selection of simulated showers and muons is identical to the one for the experimental data, and the shower energy assignment is done with the reconstructed parameters. In addition, all simulated showers fulfill the *software trigger* condition that at least 10 stations in one of the outer clusters of the KASCADE Array have a signal from e/γ detectors above the threshold. This condition is an equivalent of the experimental condition that the MTD is being triggered by the KASCADE Array.

4. Lateral muon density distributions

4.1. Description of the analysis

The geometry of a typical shower event is shown in Fig. 5. The **near** vertical shower hits the ground in the Grande Array. The core position, direction and other parameters are reconstructed with the information from the arrays of charged particles and muon detectors.

To obtain the lateral distributions of muons registered in the MTD the following procedure was applied:

1. For each shower, the distance R_μ was divided into 30-meter-wide radial bins around the reconstructed shower core position in shower coordinates.

2. In each distance bin, the number of muons was calculated using the position of the hit in the middle detector module in 3-hit tracks or extrapolation of the position of the hit to the level of the middle detector module in 2-hit tracks for each reconstructed track.

3. The calculation of the area of the detector in each distance bin is done in the following way. In a standard set of data taking two neighbouring wires are combined. With the perpendicular strip they create a 20×20 mm^2 cell that is a basic detection area in the module. With the positions of wires and strips, the location of each cell is calculated and its size added to the detector area contained in the particular R_μ bin. The area was corrected for the zenith angle of a shower multiplying it by the cosine of this angle.

The number of reconstructed muon tracks may be distorted by the data acquisition and/or trigger inefficiencies [13]. As a result, one can obtain no tracks in a distance bin even if the size of the detector area, and the registered muon density in the neighbouring bin make such a zero-track registration highly improbable. **However, when the two parts differ significantly in size the lack of muon observation in the smaller part of the detector (having typically less than 10% - 20% of the full area) may be also due to the muon number fluctuations in air showers. Including the areas without muons into the density calculations gives the true values only with the perfect detector. However, in our case, the above mentioned inefficiencies could create a strong bias of the calculated muon densities towards lower values if no special means to minimize their influence on the results were undertaken. There is a benefit of having large detectors like the MTD, where at primary energy above 10^{16} eV we should nearly always expect a muon in a bin with 50 m^2- 128 m^2 of detector area in it (typical values).**

For most of the showers the MTD was divided in two distance bins (78% of the showers) or was fully contained in one distance bin only (12% of the showers). If the two parts were of similar size the muons were usually detected in both of them. In the **remaining** 10% of the showers when the MTD was divided into three parts (three distance bins), in all cases the middle part always had muons, and one of the others, small ones, could have no muons in it.

In the analyses the bias was minimized by the selection of muon-to-shower-axis distance ranges where the fraction of cumulated detector area without muons is small due to the low probability of "no registration" both by physical and instrumental reasons. The fraction of the area without muons due to the detector inefficiencies, contributing to the systematic uncertainty of the result, was estimated in the following (section 4.2).

The density in each distance bin was calculated as a sum of all muons from all showers, corrected for reconstruction efficiency, being divided by the detector area in that distance bin, corrected for zenith angle (A_{MTD}).

$$\rho_i = \frac{\sum_{k=1}^{N_s}(N_{tr2}^{k,i} + N_{tr3}^{k,i}) \cdot \mathcal{K}}{\sum_{k=1}^{N_s} A_{MTD}^{k,i}} \quad (3)$$

where i is the distance bin number, N_s is the number of showers, $A_{MTD}^{k,i}$ is the detector area in i^{th} distance bin for the k^{th} shower, N_{tr2} **and** N_{tr3} **are the number of 2-hit and 3-hit muon tracks, respectively**, and $\mathcal{K}$ is a track reconstruction efficiency correction factor [13].

4.2. Determination of the MTD full-efficiency distance ranges

The lateral muon density distributions in EAS obtained with muon tracks were investigated in the primary CR energy range from 10^{16} eV to 1.6×10^{17} eV (in four energy sub-ranges, energy calculated with formula (1)) in the muon-to-shower-axis distance from 100 m to 700 m.

Historically, the parametrization of the measured lateral distributions was usually done with Greisen [18], NKG [19] or Lagutin [20] type lateral distribution functions (LDF). These functions describe the lateral density distributions differently in the distance range close to and far away from the shower core. The first two describe equally well the measured distributions of muon densities at different energy thresholds up to 200 m [4], the Lagutin function was applied to describe the lateral distributions in distance range 100 m – 600 m [8].

The functional relation will only describe well the measurement in the muon-to-shower-axis distance where the above mentioned inefficiencies **have no or negligible effect**. **The actual value of the efficiency, being a measure of the detector capability to register all muons which fall onto it, cannot be directly measured. However, one can indirectly, by examining various experimental quantities, find the muon-to-shower-axis distance ranges where the muon registration efficiency with the MTD has its maximum and constant value. We have called them full-efficiency distance ranges (FR) and, prior to the application of any fitting procedure, such ranges were determined for each of the four primary energy intervals, in** $\lg(E_0^{rec}$**[GeV]) equal to: 7.0 - 7.3, 7.3 - 7.6, 7.6 - 7.9 and 7.9 - 8.2.**

They are determined as the distance ranges where all of the following conditions should be fulfilled:

1. The number of showers N_s passing the shower and muon selection criteria in all 30-meter distance bins is not smaller than the mean value by more than two standard deviations[7] **– for sufficiently large muon statistics**.

2. The value of the detector area with muons A_{MTD} does not differ from the mean $\langle A_{MTD} \rangle$ by more than one standard deviation **– giving nearly constant detection area in each distance bin**.

3. The mean number of muon tracks $\langle N_{tr} \rangle = \langle N_{tr3} + N_{tr2} \rangle$ registered in the far end of the full efficiency distance range is larger than three.

4. The fraction F of showers without muons in the MTD in the whole number of KASCADE-triggered showers should **be in its plateau region**.

The third condition is introduced in order to minimize the **probability of distance bins with** detector areas without muon tracks A_0**, called *empty detector areas*, due to the muon number fluctuations**.

The forth condition allows not to consider showers without muons in the analysis **and ensures that the remaining registration inefficiencies are at minimum level**.

In Fig. 6, as an example, for the primary energy range $\lg(E_0^{rec}$[GeV])=7.3 – 7.6 the lateral distributions of the following quantities **used for the FR determination** are shown: the mean detector area with muons $\langle A_{MTD} \rangle$ (a), the mean number of muon tracks $\langle N_{tr} \rangle$ (b), the number of showers N_s (c), and the ratio of the empty detector area A_0, to the sum $A_{MTD} + A_0$ (d).

As seen in Fig. 6(d) the accumulated empty detector area increases with the distance, reaching at the far-end distance bin of the FR approx. **7%**. **This increase corresponds to the decrease of the** $\langle N_{tr} \rangle$ **(Fig. 6b) which is a strong indication that these empty areas have physical meaning and should be included in muon density calculation. However, one should estimate what is the remaining level of the detector inefficiencies contributing to the values in Fig. 6d, constituting the systematical bias of the result towards lower values and determining the value of "full efficiency". It has been done comparing the plots like in Fig. 6d and Fig. 6b for all four primary energy intervals. In all of them the plots of empty detector areas in the first two-three distance bins of the corresponding FR are showing equal and constant value on the level of 1%. By taking this into account, as well as the large values of** $\langle N_{tr} \rangle$ **there (Fig. 6b), we attributed this 1% of area to the remaining detector inefficiency effects, which are at that level in the whole FR. Therefore, our full efficiency is estimated to be on the level of 99% and the 1% bias due to the inefficiencies contributes to the systematical error of our results.**

In Table 1 the results of the determination of the MTD full-efficiency distance ranges are summarized.

Table 1: MTD full-efficiency distance ranges (FR) in four primary energy intervals.

$\lg(E_0^{rec}$[GeV])	FR [m]	$\langle N_s \rangle$	$\langle A_{MTD} \rangle$[m^2]
7.0 – 7.3	100 – 370	782±256	72±3
7.3 – 7.6	130 – 460	226±57	71±5
7.6 – 7.9	220 – 550	68±12	72±6
7.9 – 8.2	370 – 580	22±3	69±8

[7] In the two highest energy intervals – one standard deviation only.

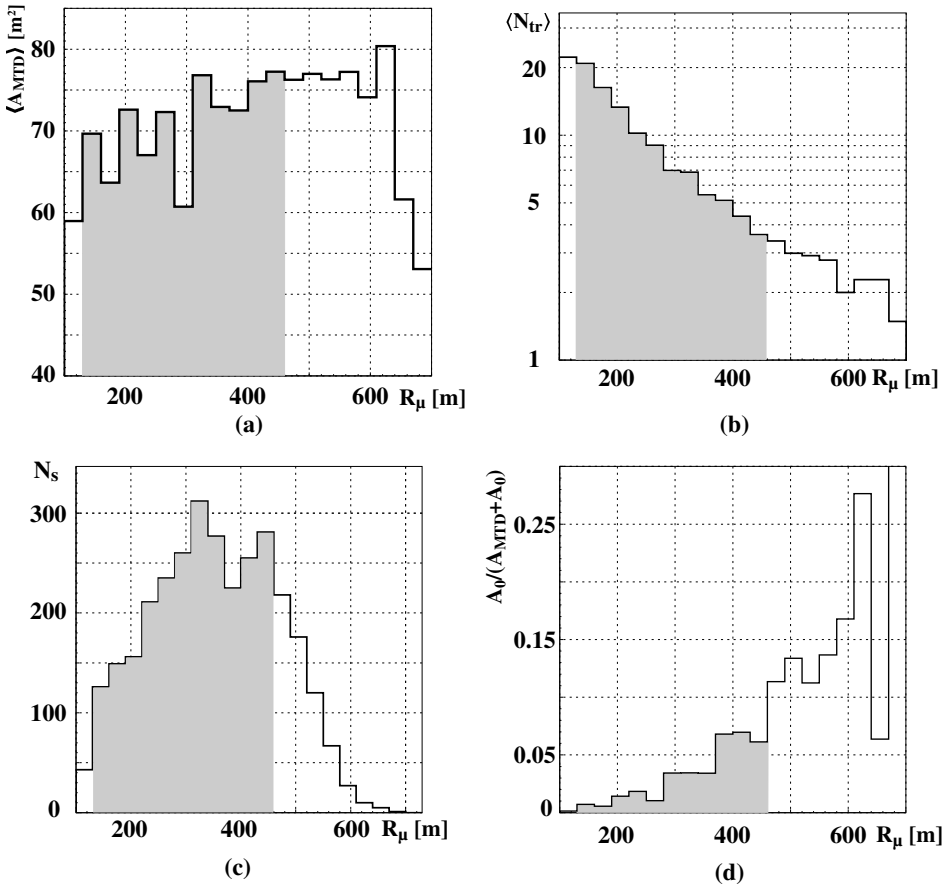

Figure 6: Lateral distributions of the following quantities for the primary energy range lg(E_0^{rec}[GeV])=7.3 − 7.6: (a)$\langle A_{MTD}\rangle$, (b) $\langle N_{tr}\rangle = \langle N_{tr3} + N_{tr2}\rangle$, (c) the number of showers N_s and (d) the ratio of the empty detector area A_0 to the sum $A_{MTD} + A_0$. Full-efficiency distance range (FR), **determined with quantities from (a), (b) and (c), as well as the information on F for this energy range (not shown),** is marked with grey area.

4.3. Results and discussion

The lateral muon density distributions in EAS obtained with muon tracks are presented in Fig. 7 **and in Table 2**. **Errors are small and could not be seen in the graphical presentation in Fig. 8. They are listed in the table only. In addition to the small statistical errors there are several sources of the systematic ones. Apart from the above mentioned 1% bias due to the remaining inefficiencies there are three other sources: accuracy in energy estimation by formula (1), resolution in shower direction and accuracy in core position determination. In the four primary energy sub-ranges above 10^{16} eV used in this work the mean error in energy given by (1) is: 24.5%, 22.2%, 20.0% and 17.9%, decreasing with energy [21]. The two other uncertainties are 0.8° and 6 m, respectively [8]. Varying individually primary energy, shower directions and core positions by these values the contribution of these uncertainties to the total systematic error of measured muon density was determined. The total systematic values are dominated by uncertainty of primary energy, being, in the FR of the MTD, on the level of ±(15 – 30)%, the core position uncertainty introduces, per average, about -3% and +14% change of the result, while the angular resolution has an influence on ±(1 – 2)% level only.**

In all energy intervals the lateral distributions obtained with the MTD are fitted with a function proposed by Greisen for the muonic component (E_μ^{thr}=1 GeV)[8] :

$$\rho(r) = C\left(\frac{r}{r_G}\right)^{-0.75}\left(1+\frac{r}{r_G}\right)^{-2.5} \quad (4)$$

where C = const. · N_μ, r_G is the Greisen radius. In this analysis the fitted parameters are r_G and the scaling factor C of the distributions.

The values of the C and r_G fit parameters are presented in Table 3. The distributions were fitted in the MTD full efficiency ranges, as determined above. In Fig. 7 the experimental MTD-points used in the fits are marked with full symbols.

It is worth to note that the LDFs become steeper with the energy of the EAS (the value of r_G is decreasing). This is due

[8] It is also well suited for our analysis because only less than 5% of muons above 800 MeV have energy below 1 GeV. Moreover, our effective threshold is slightly higher because muons are mostly not vertical ($\langle\theta\rangle \approx 13.3° \pm 0.2°$)

Table 2: Densities of muons with their statistical and systematic errors obtained with the MTD in four primary particle energy ranges and distance range 100 m – 610 m. Values in bold are used to fit the Greisen functions.

Middle of the distance range [m]	ρ [m^{-2}] $\pm\sigma_{stat} \pm \Delta_{syst}$ lg(E_0^{rec}[GeV]): 7.0 - 7.3	7.3 - 7.6	7.6 - 7.9	7.9 - 8.2
115	**0.228 ± 0.002** $^{+0.063}_{-0.054}$	0.369 ± 0.004 $^{+0.053}_{-0.041}$	0.58 ± 0.02 $^{+0.04}_{-0.16}$	0.24 ± 0.08 $^{+0.40}_{-0.25}$
145	**0.167 ± 0.001** $^{+0.050}_{-0.042}$	**0.314 ± 0.003** $^{+0.071}_{-0.076}$	0.469 ± 0.009 $^{+0.065}_{-0.042}$	0.63 ± 0.04 $^{+0.01}_{-0.63}$
175	**0.131 ± 0.001** $^{+0.038}_{-0.030}$	**0.249 ± 0.002** $^{+0.054}_{-0.053}$	0.424 ± 0.006 $^{+0.065}_{-0.068}$	0.56 ± 0.03 $^{+0.11}_{-0.16}$
205	**0.105 ± 0.001** $^{+0.031}_{-0.023}$	**0.197 ± 0.002** $^{+0.053}_{-0.040}$	0.364 ± 0.005 $^{+0.078}_{-0.062}$	0.49 ± 0.02 $^{+0.03}_{-0.03}$
235	**0.087 ± 0.001** $^{+0.026}_{-0.019}$	**0.164 ± 0.002** $^{+0.047}_{-0.035}$	**0.309 ± 0.005** $^{+0.040}_{-0.067}$	0.47 ± 0.02 $^{+0.01}_{-0.07}$
265	**0.071 ± 0.001** $^{+0.021}_{-0.017}$	**0.137 ± 0.001** $^{+0.037}_{-0.027}$	**0.262 ± 0.004** $^{+0.041}_{-0.056}$	0.43 ± 0.01 $^{+0.01}_{-0.06}$
295	**0.056 ± 0.000** $^{+0.017}_{-0.012}$	**0.113 ± 0.001** $^{+0.026}_{-0.025}$	**0.204 ± 0.004** $^{+0.033}_{-0.040}$	0.37 ± 0.01 $^{+0.09}_{-0.08}$
325	**0.045 ± 0.000** $^{+0.013}_{-0.009}$	**0.093 ± 0.001** $^{+0.024}_{-0.023}$	**0.177 ± 0.003** $^{+0.045}_{-0.035}$	0.359 ± 0.009 $^{+0.059}_{-0.056}$
355	**0.038 ± 0.000** $^{+0.010}_{-0.008}$	**0.074 ± 0.001** $^{+0.022}_{-0.018}$	**0.142 ± 0.003** $^{+0.028}_{-0.032}$	0.297 ± 0.008 $^{+0.052}_{-0.078}$
385	0.033 ± 0.000 $^{+0.008}_{-0.006}$	**0.062 ± 0.001** $^{+0.015}_{-0.014}$	**0.107 ± 0.002** $^{+0.028}_{-0.019}$	**0.215 ± 0.006** $^{+0.039}_{-0.032}$
415	0.029 ± 0.000 $^{+0.007}_{-0.007}$	**0.054 ± 0.001** $^{+0.013}_{-0.014}$	**0.104 ± 0.002** $^{+0.020}_{-0.021}$	**0.188 ± 0.006** $^{+0.058}_{-0.041}$
445	0.024 ± 0.001 $^{+0.006}_{-0.006}$	**0.043 ± 0.001** $^{+0.010}_{-0.009}$	**0.088 ± 0.002** $^{+0.013}_{-0.024}$	**0.140 ± 0.005** $^{+0.042}_{-0.041}$
475	0.021 ± 0.001 $^{+0.007}_{-0.006}$	0.038 ± 0.001 $^{+0.010}_{-0.008}$	**0.070 ± 0.002** $^{+0.012}_{-0.015}$	**0.126 ± 0.005** $^{+0.020}_{-0.030}$
505	0.018 ± 0.001 $^{+0.007}_{-0.006}$	0.036 ± 0.001 $^{+0.007}_{-0.008}$	**0.066 ± 0.002** $^{+0.017}_{-0.018}$	**0.118 ± 0.004** $^{+0.028}_{-0.024}$
535	0.016 ± 0.001 $^{+0.006}_{-0.007}$	0.030 ± 0.001 $^{+0.007}_{-0.005}$	**0.054 ± 0.002** $^{+0.008}_{-0.012}$	**0.119 ± 0.005** $^{+0.039}_{-0.033}$
565	0.014 ± 0.002 $^{+0.003}_{-0.002}$	0.027 ± 0.001 $^{+0.006}_{-0.010}$	0.044 ± 0.002 $^{+0.008}_{-0.008}$	**0.088 ± 0.004** $^{+0.031}_{-0.016}$
595	0.013 ± 0.003 $^{+0.005}_{-0.006}$	0.021 ± 0.002 $^{+0.004}_{-0.007}$	0.040 ± 0.002 $^{+0.014}_{-0.008}$	0.081 ± 0.004 $^{+0.016}_{-0.019}$

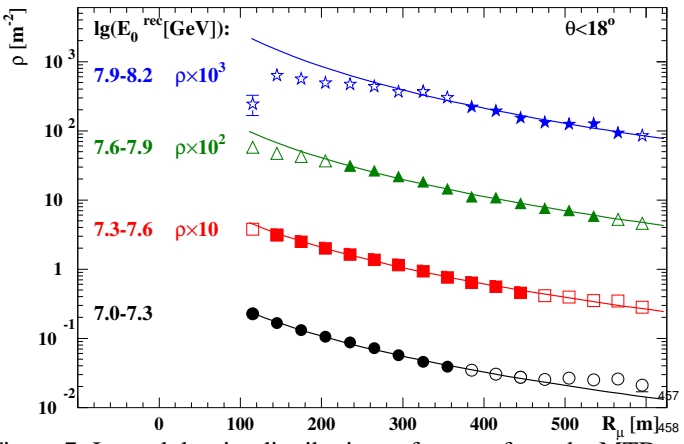

Figure 7: Lateral density distributions of muons from the MTD in four primary energy ranges. The distributions can be described by the Greisen function in the distance ranges (FR) marked with full symbols. **Errors - see Table 2.**

Table 3: Fit parameters C and r_G of the lateral density distributions of muons obtained with the MTD.

lg(E_0^{rec}[GeV])	C[m^{-2}]	r_G[m]	χ^2/NDF
7.0 – 7.3	0.151±0.006	441±10	19/7
7.3 – 7.6	0.30±0.02	434±14	14/9
7.6 – 7.9	1.0±0.1	325±15	5/9
7.9 – 8.2	3.4±0.6	247±19	4/5

to the fact that with increasing energy the shower penetrates deeper into the atmosphere. The same behaviour was observed for muon and electron LDFs in the KASCADE Array [4].

It has been observed, especially seen in the 3rd and 4th energy range, that the LDFs for the KASCADE Array (E_μ^{thr}=230 MeV) are flatter than the LDFs for the MTD muons (E_μ^{thr}=800 MeV) confirming the known dependence of the r_G value in Greisen's formula on the muon energy threshold. This is related to the decrease of the muon parent production angle ($\theta_\pi \simeq p_t/E$) with muon energy and to the weaker multiple Coulomb scattering ($\theta_s \propto 1/E_\mu$).

The shape of the lateral muon density distributions in those distances selected for the Greisen fits allows **fitting** them equally well also with a Lagutin-type function.

For instance, in the first energy bin, the MTD distribution has been fitted with the Greisen function in the distance range from 100 m to 370 m. At larger distances the MTD distribution is rising, as well as the uncertainty of the density values due to decreasing number of showers and muons there. In the last energy bin, the MTD distribution was fitted with the Greisen function in the distance range from 370 m to 580 m. In distances outside this range the MTD distribution gives lower (<370 m) or higher (>580 m) values than predicted by the Greisen function, and the uncertainties of the densities are increasing.

Outside the MTD full-efficiency distance ranges the deviations of the experimental points from the Greisen type functional dependence are seen due to the various inefficiencies discussed above. They are responsible for the shape of the MTD muon lateral density distributions at large distances

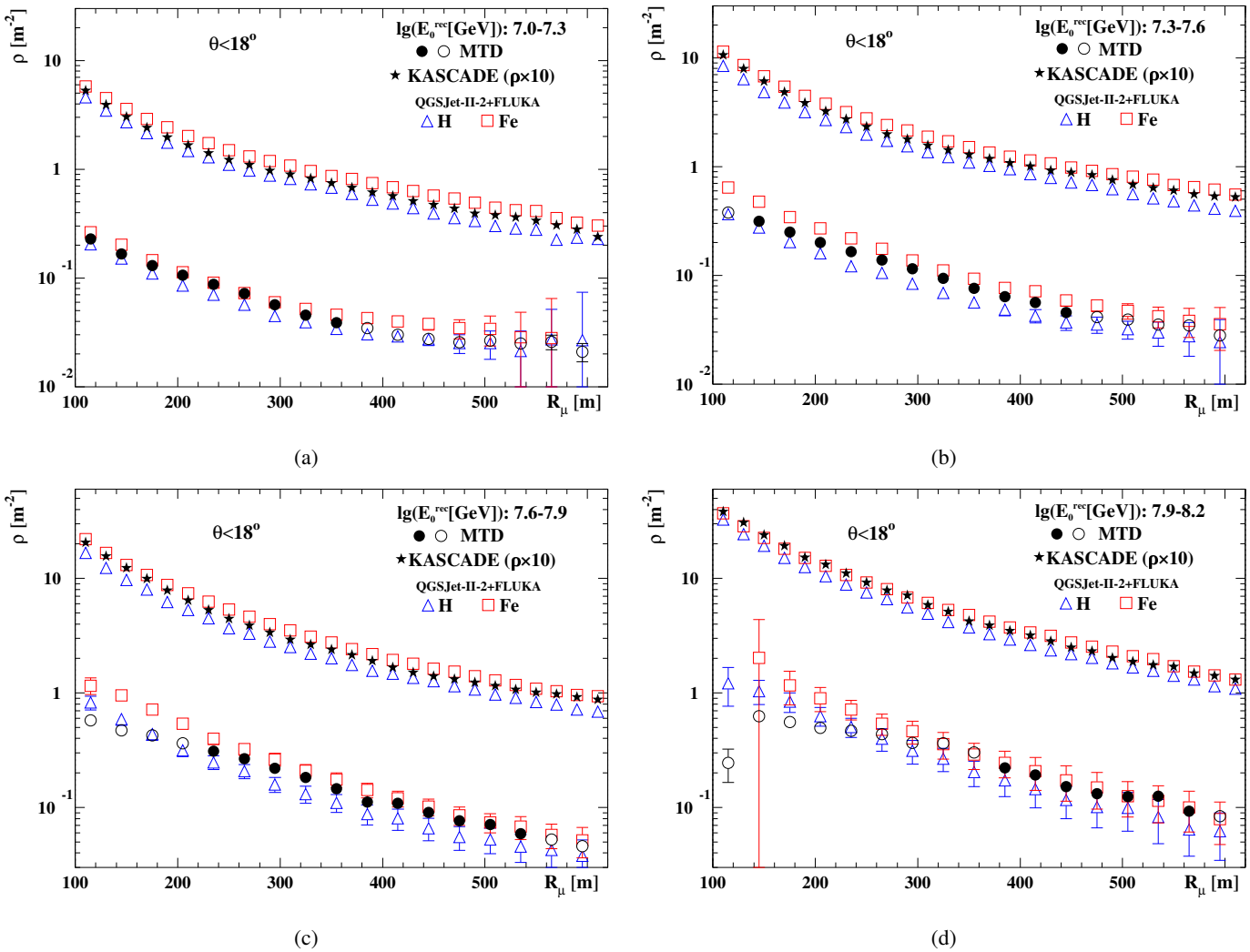

Figure 8: Lateral muon density distributions obtained with the MTD (E_μ^{thr}**=800 MeV)** (•, ○) and KASCADE Array measurements **(**E_μ^{thr}**=230 MeV)** (★) together with CORSIKA simulations (△, □) in the primary energy ranges: (a) lg(E_0^{rec}[GeV])=7.0 – 7.3, (b) lg(E_0^{rec}[GeV])=7.3 – 7.6, (c) lg(E_0^{rec}[GeV])=7.6 – 7.9, (d) lg(E_0^{rec}[GeV])=7.9 – 8.2. The lateral distributions obtained with the KASCADE Array are multiplied by factor 10. **Only some statistical errors in the simulations can be seen.**

changing the population of showers with muon tracks reconstructed with the MTD in that distance range.

4.4. Comparison with lateral density distributions from simulations and KASCADE Array

For the purpose of testing the interaction models used in the EAS simulations the comparisons of the experimental muon density distributions at two energy thresholds, obtained with the MTD and with the KASCADE Array, with simulated ones have been done. Simulations were performed for H and Fe primary initiated showers using CORSIKA with QGSJet-II-2+FLUKA2002.4 hadronic interaction models. The results are shown in Fig. 8.

In all energy bins the presented simulations reproduce the experimental distributions within error bars in the sense that the experimental data is bracketed by the simulations with proton and iron primaries, i.e. no unexpected physical processes are visible. However, in case of the MTD distributions, in the distance range up to 200 m (clearly visible in the 3rd and 4th energy bin) the densities for simulations are higher than the densities for the measurement. This **is probably due to** the idealized description of the MTD in the detector simulation code that "fails" in reproducing the detector behaviour in extreme cases of high muon density events, when the saturation of the data acquisition and overlapping hit clusters occur.

Further tests of hadronic interaction models can be done by calculating the ratios of the muon densities obtained for different threshold energies. By investigating such a ratio a sensitivity to the muon energy spectrum in high-energy air showers could be achieved. However, due to the small differences in the muon densities between proton and iron

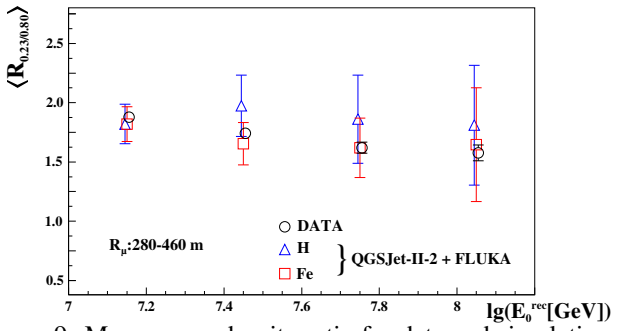

Figure 9: Mean muon density ratio for data and simulations at the distance from 280 m to 460 m at two energy thresholds as a function of the shower energy. The points are shifted for better visibility. Only statistical errors are shown.

initiated showers, as well as the experimental uncertainties it is difficult to extract a parameter which is both, sensitive to composition and the validity of the hadronic interaction model.

In earlier analyses of the R_{ρ_1/ρ_2}=f(lg E) dependence described in Refs. [22, 23, 24], the muon density ratios for different energy thresholds measured in KASCADE were investigated (e.g. $R_{2.4/0.49}=\rho_{2.4}/\rho_{0.49}$, $R_{0.49/0.23}=\rho_{0.49}/\rho_{0.23}$). Those investigations were done in the energy range lg(E_0^{rec}[GeV])=6.0 – 7.0 and in the distance from 30 m to 70 m. Comparison of several hadronic interaction model combinations (e.g. QGSJet1998+GHEISHA) with the data revealed significant differences between the distributions of the density ratios. The conclusion was that the simulations could not describe well the measurements, but a more detailed quantification was hampered by experimental and methodical uncertainties.

In this analysis we investigate $R_{0.23/0.8}$, the ratio of $\rho_{0.23}$ and $\rho_{0.8}$ which are the densities of muons with energy above 0.23 GeV from the KASCADE and 0.8 GeV from the MTD, and its dependence on shower energy $R_{0.23/0.8}$=f(lg(E_0^{rec})).

In Fig. 9 the dependence of the mean muon density ratio calculated with the mean densities in R_μ distance from 280 m to 460 m (see Figure 7) in four energy intervals is shown.

The decrease of the mean density ratio for data is of the order of 10% per decade of the shower energy, however with large statistical errors. A similar decrease can be observed in the simulations where the ratios for iron showers follow the ratios from the measurement. **Due to the above mentioned limitations we cannot judge on the significance of this observation, however, this** behaviour shows the trend similar to other investigations of the mass composition at KASCADE-Grande, which indicate that at these energies the composition is significantly heavier than proton **[25], [26]**.

The presented $R_{0.23/0.8}$ analysis indicates only that, as in the case of lateral muon distributions, the description of the experimental data by the simulations with QGSJet-II-2+FLUKA2002.4 model combination does not require inclusion of any exotic processes. A more detailed quantification, similarly as in the previous density ratio investigations in KASCADE, is impossible due to the experimental uncertainties.

5. Summary and conclusions

Employing the large and precise muon tracking device in KASCADE-Grande the use of the tracking technique for the muon lateral distribution measurements has been revived. For the first time the lateral density distributions of EAS muons (E_μ^{thr}=800 MeV) have been obtained by counting muon tracks for radial distance 100 m – 610 m, in four primary energy ranges above 10^{16} eV and with high statistical accuracy.

The obtained results validate the excellent performance of the MTD, which has already delivered valuable results on the muon production heights, cosmic ray composition and model tests [27, 28, 29].

The MTD distributions can be described with the Greisen function, however in a limited distance range, different for each energy interval. This is due to the limited efficiency of track reconstruction in the MTD, caused by the saturation of the detector, as well as by trigger inefficiency.

The LDFs from the MTD become steeper with the energy of the showers. The same behaviour was observed for the muon and electron LDFs obtained with the KASCADE Array, as shown in Ref [4]. The dependence of the shape of lateral muon distribution (r_G value in Greisen's formula) on muon threshold energy was observed.

The lateral distributions obtained with the MTD are compared with the density distributions based on energy deposits obtained with the KASCADE Array of scintillator detectors (E_μ^{thr}=230 MeV) for the same sample of EAS. The measured distributions are compared with distributions in simulated showers, QGSJet-II-2+FLUKA2002.4 model combination, Hydrogen and Iron initiated EAS. The comparisons of the lateral muon density distributions, as well as of the density ratio $R_{0.23/0.8}$ show that the MTD and KASCADE results are bracketed by the simulated distributions i.e. no unexpected physical processes are visible. This indicates that the hadronic interaction models have been significantly improved because the simulations performed with earlier models, like QGSJet1998+GHEISHA, could not describe the KASCADE air shower data.

Acknowledgements

The authors would like to thank the members of the engineering and technical staff of the KASCADE-Grande collaboration, who contributed to the success of the experiment. The KASCADE-Grande experiment is supported in Germany by the BMBF and by the Helmholtz Alliance for Astroparticle Physics - HAP funded by the Initiative and Networking Fund of the Helmholtz Association, by the MIUR and INAF of Italy, the Polish Ministry of Science and Higher Education, and the Romanian National Authority for Scientific Research, CNCS - UEFISCDI, project number PN-II-ID-PCE-2011-3-0691 and PN-II-RU-PD-2011-3-0145.

[1] T. Pierog, EPJ Web Conf. 52 (2013) 03001.
[2] L. Pentchev, P. Doll, H. O. Klages, J. Phys. G 25 (1999) 1235.
[3] L. Pentchev, P. Doll, J. Phys. G 27 (2001) 1459.
[4] T. Antoni, et al. (The KASCADE Collaboration), Astropart. Phys. 14 (2001) 245–260.
[5] W. Apel, et al. (KASCADE-Grande Collaboration), Astropart. Phys. 24 (2006) 467 – 483.

[6] F. Ashton, J. Fatemi, H. Nejabat, A. Nasri, W. S. Rada, E. Shaat, A. C. Smith, T. R. Stewart, M. G. Thompson, M. W. Treasure, I. A. Ward, in: Proc. 15^{th} ICRC, 1977, volume 11, Plovdiv, Bulgaria, p. 400.
[7] M. Samorski, W. Stamm, in: Proc. 18^{th} ICRC, 1983, Bangalore, India.
[8] W. D. Apel, et al. (The KASCADE-Grande Collaboration), Nucl. Instrum. Meth. A 620 (2010) 202–216.
[9] T. Antoni, et al. (KASCADE Collaboration), Nucl. Instrum. Meth. A 513 (2003) 490–510.
[10] P. Doll, W. Bartl, C. Büttner, K. Daumiller, K.-H. Kampert, H. Klages, D. Martello, R. Obenland, L. Pentchev, J. Zabierowski, Nucl. Instrum. Meth. A 488 (2002) 517 – 535.
[11] W. Apel, et al., Astropart. Phys. 29 (2008) 412–419.
[12] J. Zabierowski, P. Doll, Nucl. Instrum. Meth. A 484 (2002) 528–532.
[13] P. Łuczak, "Investigation of muons in extensive air showers with the KASCADE-Grande Muon Tracking Detector", Ph.D. thesis, National Centre for Nuclear Research, Poland, 2012. http://www.ncbj.gov.pl/node/1951.
[14] M. Bertaina, et al. (KASCADE-Grande Collaboration), in: Proc. 31^{th} ICRC, 2009, Lodz, Poland. FZKA 7516, p13-16 (0323).
[15] D. Heck, et al., "CORSIKA: a Monte Carlo code to simulate extensive air showers", Technical Report 6019, Forschungszentrum Karlsruhe(FZKA), 1998.
[16] S. Ostapchenko, Nucl. Phys. B (Proc. Suppl.) 151 (2006) 143–146.
[17] A. Ferrari, P.R. Sala, A. Fasso, and J. Ranft, "FLUKA: a multi-particle transport code", Technical Report, CERN, 2005. CERN-2005-010 ; INFN-TC-2005-11 ; SLAC-R-773.
[18] K. Greisen, Ann. Rev. Nuc. Sci. 10 (1960) 63–108.
[19] K. Kamata, J. Nishimura, Prog. Theor. Phys. Suppl. 6 (1958) 93–155.
[20] A. A. Lagutin, A. V. Pljasheshnikov, V. V. Uchaikin, in: Proc. 16^{th} ICRC, 1979, volume 7, Kyoto, Japan, p. 18.
[21] W. D. Apel, et al., Astroparticle Physics 36 (2012) 183 – 194.
[22] A. Haungs, et al., Nucl. Phys. B (Proc. Suppl.) 151 (2006) 167 – 174.
[23] A. Haungs, et al. (The KASCADE Collaboration), in: Proc. 28^{th} ICRC, 2003, Tsukuba, Japan. FZKA 6890 p.37-40.
[24] A. Haungs, et al. (The KASCADE-Grande Collaboration), in: Proc. 29^{th} ICRC, 2005, volume 6, Pune, India, pp. 281–284.
[25] W. D. Apel, et al. (KASCADE-Grande Collaboration), Phys. Rev. Lett. 107 (2011) 171104.
[26] W. D. Apel, et al., Astroparticle Physics 47 (2013) 54 – 66.
[27] W. Apel, et al. (KASCADE-Grande Collaboration), Astropart. Phys. 34 (2011) 476 – 485.
[28] P. Łuczak, et al. (KASCADE-Grande Collaboration), in: Proc. 33^{rd} ICRC, 2013, Rio de Janeiro, Brasil. arXiv:1308.2059.
[29] J. Zabierowski, et al. (KASCADE-Grande Collaboration), in: Proc. 30^{th} ICRC, 2007, volume 4, Merida, Mexico, pp. 111–114.